Numerical analysis of flow within a packed bed using computational fluid dynamics: Effects of fluid nature and regime

Soufyane Ladeg[1,2] and Nadji Moulai-Mostefa[2]

[1]*FST, University of Tissemsilt, Tissemsilt, Algeria*
[2]*LME, University of Medea, Medea, Algeria*

Abstract

This research conducts a computational fluid dynamics (CFD) analysis comparing laminar and k-epsilon turbulent models of fluid flow through a packed bed. For this, three types of fluids (water, water vapor and carbon dioxide) were examined. The CFD model was initially juxtaposed with two experimental ones reported in the literature. It was observed that the numerical model used was in reasonable agreement with the experimental data reported in literature, provided that the packed bed dimensions (column diameter and height, grain size) aligned with those used experimentally. Thus, a decrease in pressure in descending order was noticed for the three fluids studied for both regimes from the column top to the outlet. In addition, a thorough characterization of turbulence was conducted, including determination of turbulent kinetic energy (TKE) and turbulent eddy dissipation (TED). As a result, a rapid dissipation of TKE for water was observed compared to the other two fluids, where TKE decreased progressively along the column length. In contrast, the TED for water decreases gradually until the exit of the column, while for both gaseous fluids, it increases slowly along the column length. The analysis of the vapor flow included testing of two density models, namely the constant density and the Peng-Robinson model. It was observed that the PR model for vapor properties showed similar trends of TKE and TED as those predicted for carbon dioxide.

Keywords: Fixed bed, flow pattern, turbulence, modelling.

Available on-line at the Journal web address: http://www.ache.org.rs/HI/

1. INTRODUCTION

Due to the diminishing oil reservoirs and the completion of initial and subsequent life cycles of existing reserves, enhanced oil recovery (EOR) techniques have become crucial. Extracting oil from petroleum reservoirs in the second stage is achieved by injecting water or gas into the reservoirs [1,2]. Thus, studies of the flow of different fluids in porous soil, catalytic refining, and membrane filtration are parts of a very wide field of research [3,4].

Theory for studying single-phase laminar flow of fluids through a porous medium is based on Darcy's experiments [5]. However, its quantitative description is very complex; it moves from a saturated environment to an unsaturated one due to variations in the fluid state during flow [6,7]. There are, thus, complex relationships between the different flow parameters. Consequently, the formulation and solution of unsaturated flow problems require general analysis methods based on experimental approaches and modeling of the test results [8]. Understanding the physical phenomena linked to single- or two-phase flows at such small scales is fundamental. Indeed, interfacial phenomena and the role of intermolecular edges are still poorly understood [9]. Depending on the practical situation considered, there may exist two-phase liquid-liquid or liquid-gas flows, or even in some cases, three-phase fluid flows (liquid-liquid-gas) [10,11]. In each case, pressure loss is an important parameter to characterize the energy necessary for circulation of these fluids in a pore space. Direct measurements are difficult because experimental studies of transport mechanisms in porous media are expensive and exhibit low levels of spatial and temporal resolution. In recent years, researchers have employed numerical simulations to solve or unveil the phenomena governing the flow of fluids through a porous medium [12,13]. In this sense, computational fluid dynamics (CFD) provides possibilities to

Corresponding author: Soufiane Ladeg, Science and Technology Department, University of Tissemsilt, Tissemsilt, Algeria
E-mail: soufiane.ladeg@univ-tissemsilt.dz; https://orcid.org/0000-0003-1133-827X
Co-author: Nadji Moulai-Mostefa https://orcid.org/0000-0003-2263-025X

1

systematically reduce trials, integrate new functionalities, and optimize process time and calculation methods [14]. Additionally, it enables prediction of anomalies [15-17].

Several models were proposed to predict physical properties that governed the behavior of the fluid flow through a packed bed. A 3D two-phase flow transient Eulerian-Eulerian model was developed to evaluate liquid dispersion in a study of structured packing for gas-liquid reactions [18]. It was reported that elevating the inlet velocity results in broader dispersion of liquid. This implies that employing multiple liquid inlets, as opposed to a single one, caused an escalation in liquid hold-up. On the other hand, Wang *et al.* [19] conducted a study on hydrodynamic characteristics of a packed column using structured sinusoidal corrugated sheet packings. Their simulation study contributes to the evaluation and optimization of multiphase flow characteristics and the mass transfer performance of packed columns. CFD was used to evaluate axial dispersion properties of a fixed-bed reactor with various packed configurations with the aim To obtain the optimum design and scaling up of reactors with porous packed structures [20]., Also, direct numerical simulations (DEM-OpenFOAM workflow) was used to predict the accurate axial Peclet numbers and assess dispersion of single laminar phase flow in small fixed-bed reactors [21]. Pashchenko *et al.* [22] studied how a fluid moves in a fixed-bed reactor filled with porous particles by using both experiments and computer simulations. Their findings indicated that the flow through the porous medium of particles is minimal if the pore size is less than 0.5 mm, while it appears at the larger pore sizes. A comprehensive two-dimensional (2D) model was developed to simulate flow behavior in a fixed-bed reactor for production of olefins [23]. The model incorporated an exponential-function kinetic model, based on a lumped-species reaction scheme, into a commercial CFD code using user-defined functions. The simulation results demonstrated a close relationship between methanol conversion and catalytic deactivation, highlighting the significant influence of the operating conditions. In another study [24] a new wire gauze structured packing (PACK-2100) was found to improve mass transfer efficiency. These experiments and simulations showed better height equivalent to a theoretical plate value than conventional packings. DEM-CFD simulations were also used to study fluid flow and residence time distribution (RTD) in randomly packed beds [25] demonstrating that simulations could reliably replace some physical experiments.

The principal aim of the present research was to examine the hydrodynamic behavior of fluid flow through a packed bed using CFD. This study specifically concentrates on evaluating the pressure drop, kinetic energy dissipation, and turbulence characteristics associated with several fluid types *i.e.* water, water vapor, and CO_2. These fluids were chosen due to their prevalent applications in EOR, in-situ soil remediation, and diverse filtration processes. By offering comprehensive insights into flow dynamics within packed beds, this research seeks to enhance optimization of industrial operations through a more profound understanding of fluid behavior at the pore scale.

2. THEORY

2. 1. Mathematical formulations

Pressure drop as a process driving force is frequently employed in industry as a criterion because it is simple to measure in practice and depends on the fluid's velocity gradient [26]. However, this criterion does not enable local identification of the system regions with the greatest energy loss; it only indicates the system's total energy degradation. Ergun's equation presented by Eq. (1) is commonly used to model the pressure drop of a fluid flowing through a packed bed [27,28] and can be used for both liquids and gases. The first term of the equation corresponds to the Blake-Kozeny equation for laminar flow, while the second term corresponds to the Burke-Plummer Equation (1) for turbulent flow [29].

$$\frac{|\Delta P|}{L} = \frac{150\mu(1-\varepsilon)^2}{d_p^2\varepsilon^3}u_0 + \frac{1.75\rho(1-\varepsilon)^2}{d_p\varepsilon^3}u_0^2 \tag{1}$$

where ΔP is the pressure drop over the bed depth or length L, μ is the dynamic viscosity of the fluid, d_p is the mean particle diameter, ε is the void fraction and u_0 is the linear velocity related to the empty cross-section of the column.

The Darcy equation, also used for flows through porous media, is homogenous with the Blake-Kozeny equation for laminar flows. To determine the flow regime within the porous media, the Reynolds number is generally used in the form shown in Equation (2) [30].

$$Re = \frac{\rho d_p u_{in}}{\mu(1-\varepsilon)} \qquad (2)$$

where u_{in} is the interstitial velocity and ρ is the density of the fluid. The interstitial velocity is obtained by using the Dupuit-Forchheimer hypothesis, Equation (3), [31]:

$$u_{in} = \frac{u_0}{\varepsilon} \qquad (3)$$

Consequently, Equaton (2) can be written as Equation (4):

$$Re = \frac{\rho d_p u_0}{\varepsilon \mu(1-\varepsilon)} \qquad (4)$$

Experimental results demonstrated that the non-Darcy flow occurs at Re = 10 to 1000 in unconsolidated porous media and at Re = 0.4 to 3 in weakly consolidated rocks, according to the Chilton and Colburn's definition of the Reynolds number [30]. The inertial loss coefficient (α) can be evaluated by Equation (5) [32]:

$$\alpha = \frac{d_p^2 \varepsilon^3}{150(1-\varepsilon)^2} \qquad (5)$$

Moreover, the inertial resistance coefficient (C_2) is obtained by using Equation (6) [32]:

$$C_2 = \frac{3.5(1-\varepsilon)}{d_p \varepsilon^3} \qquad (6)$$

In the CFD model, the viscous resistance coefficient (($1/\alpha$) / m^{-2}) and the inertial resistance coefficient (C_2 / m^{-1}) are specified in each direction of the packed bed. According to previous work [33], the average particle diameter and porosity of a sand bed are d_p= 0.238 mm and ε = 0.4, respectively.

2. 2. Flow regime

Fluid simulation software ANSYS Fluent (ANSYS Inc., USA) provides powerful turbulence models, such as the Reynolds-averaged Navier-Stokes (RANS) equations coupled with turbulence models like the k-epsilon or k-omega models, to accurately simulate and analyze turbulent flows [34]. In the present study, the k-epsilon model was utilized. Laminar flow is smooth and orderly, with predictable patterns and well-defined streamlines. Therefore, the appropriate flow regime depends on the application and desired accuracy level. Turbulent flow simulations capture complex phenomena like flow separation, turbulence-induced mixing, and pressure losses, while laminar flow simulations are suitable for smooth and predictable situations. Consequently, by modeling and analyzing flow regimes, engineers and researchers can gain valuable insights into fluid behavior, identify potential instabilities, and optimize designs to enhance efficiency and performance.

2. 3. Mesh and geometry

The laboratory column, shown in Figure 1, is cylindrical (150 mm in length, 25 mm in diameter), and a corresponding 3-D cylindrical shape was created in the ANSYS Fluent interface. As a result, a well-structured mesh (hexahedral dominant meshes) is obtained with cell refinements using the ANSYS-FLUENT workbench. The meshing process involves discretizing the domain into small, interconnected elements that accurately represent the geometry and capture the flow physics. A structured mesh is advantageous as it offers several benefits. Firstly, it provides better control over element size and distribution, allowing for a more precise representation of the geometry and flow characteristics [35].

Also, a structured mesh typically requires fewer elements compared to an unstructured mesh to achieve a similar level of accuracy. To gain time in finding the meshing solution, a structural mesh with 997470 elements and 1032914 nodes was selected (Table 1). It was clearly noticed that up to those numbers of nodes and mesh elements, the pressure drop remained constant, indicating stability of the solution for mesh variations. Furthermore, the same number of elements and nodes was used in several reported studies [15,36]. In addition, a mesh of 100,000 elements is considered as a coarse mesh, while that with more than 500,000 elements is a fine mesh.
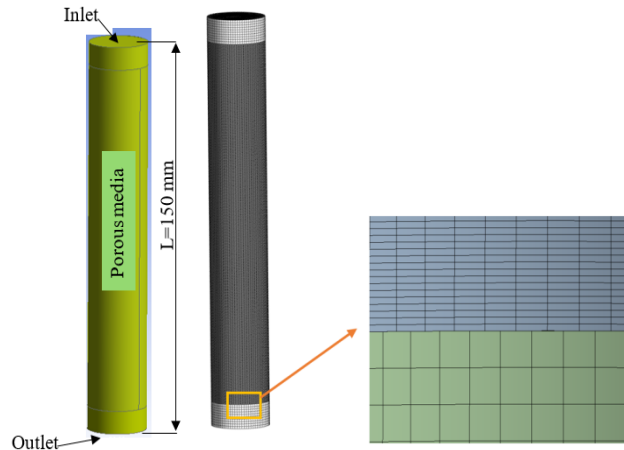
Figure 1. *Column representation showing dimensions and CFD model with meshing*

Table 1. *Mesh variation study versus pressure drop*

Run	Number of nodes	Number of mesh elements	Pressure drop, Pa
1	1032914	997470	2.34 10^4
2	1053320	1013243	2.34 10^4
3	1344520	1299180	2.34 10^4
4	2227284	2165076	2.34 10^4

The numerical solution was carried out using a pressure-based solver in ANSYS Fluent, with the simple algorithm employed for pressure-velocity coupling. For this, a second-order upwind discretization was applied to the momentum equations to enhance the accuracy of the results. Furthermore, the convergence was ensured by setting a residual tolerance of 10^{-6} and by verifying the stability and consistency of key flow parameters throughout the domain.

3. RESULTS AND DISCUSSION

3. 1. Pressure drop variation

Figure 2 compares CFD modeling results and experimental data from the literature [37,38] on pressure variation *versus* velocity. The values obtained by CFD for velocities lower or equal to 0.04 m s^{-1} are very close to the experimental results of Yang *et al.* [37]. However, for higher velocity values, there is little deviation. On the other hand, the experimental results of Erdim *et al.* [38] are well below the values predicted by CFD almost in the whole velocity range. This can be explained by the differences in column dimensions and particle sizes.
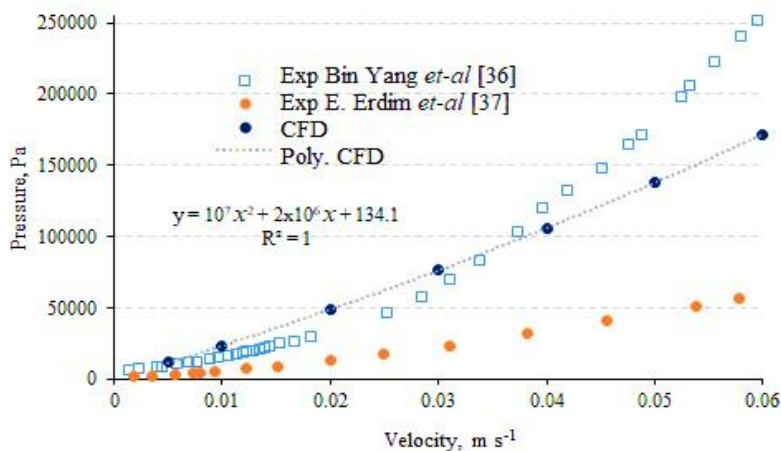

Figure 2. *Pressure vs. velocity values (symbols) obtained experimentally and by CFD modeling; line represents the best polynomial fit of the CFD data given by the presented equation; experimental data are reprinted with permission from Yang et al. [37] for 6 mm particles and 0.4 bed porosity and Edim et al. [38] for 1.18 mm glass spheres and 0.377 bed porosity*

In the first study [37], the authors used dimensions similar to the CFD model: 200 mm long column, 40 mm in diameter, with a particle diameter of 6 mm and the porosity of 0.4 . In contrast, in the second study [38] the column was 2000 mm in height and 40.14 mm in diameter, while the size of glass spheres used for the data shown in Figure 2 was 1.18 mm with the bed porosity of 0.377. Thus, the interpretation of the results indicates a relatively good agreement between CFD and experimental results at low velocities, while considerable discrepancies are observed at higher velocities due to different columns and particle dimensions. However, regardless of whether the results are obtained experimentally or through CFD simulations, the essential feature is the parabolic shape of the curve observed in all cases.

Figure 3 presents the pressure variation along the column for the three fluids. The pressure profiles across the packing are nearly linear for all fluid types. It is discernible that, at the velocity of 0.01 m s^{-1} at laminar flow conditions, due to the resistance of the porous media, there is a significant pressure drop from the top to the bottom [39]. The CFD outcomes were juxtaposed with the projections derived from the theoretical model, embodied by the Ergun equation for the laminar segment. As observed, a reasonable concurrence exists between the anticipated values from both CFD and the theoretical model. In essence, despite disparities observed in the analytical model concerning water, CO_2, and water vapor, a well-constructed mesh in the CFD model adeptly correlates with the theoretical model under laminar flow conditions. The analytical model closely corresponds with the CFD model for water while displaying a minor deviation for CO_2 and vapor. Discrepancy can be effectively resolved by adjusting the density of the modeled fluids.
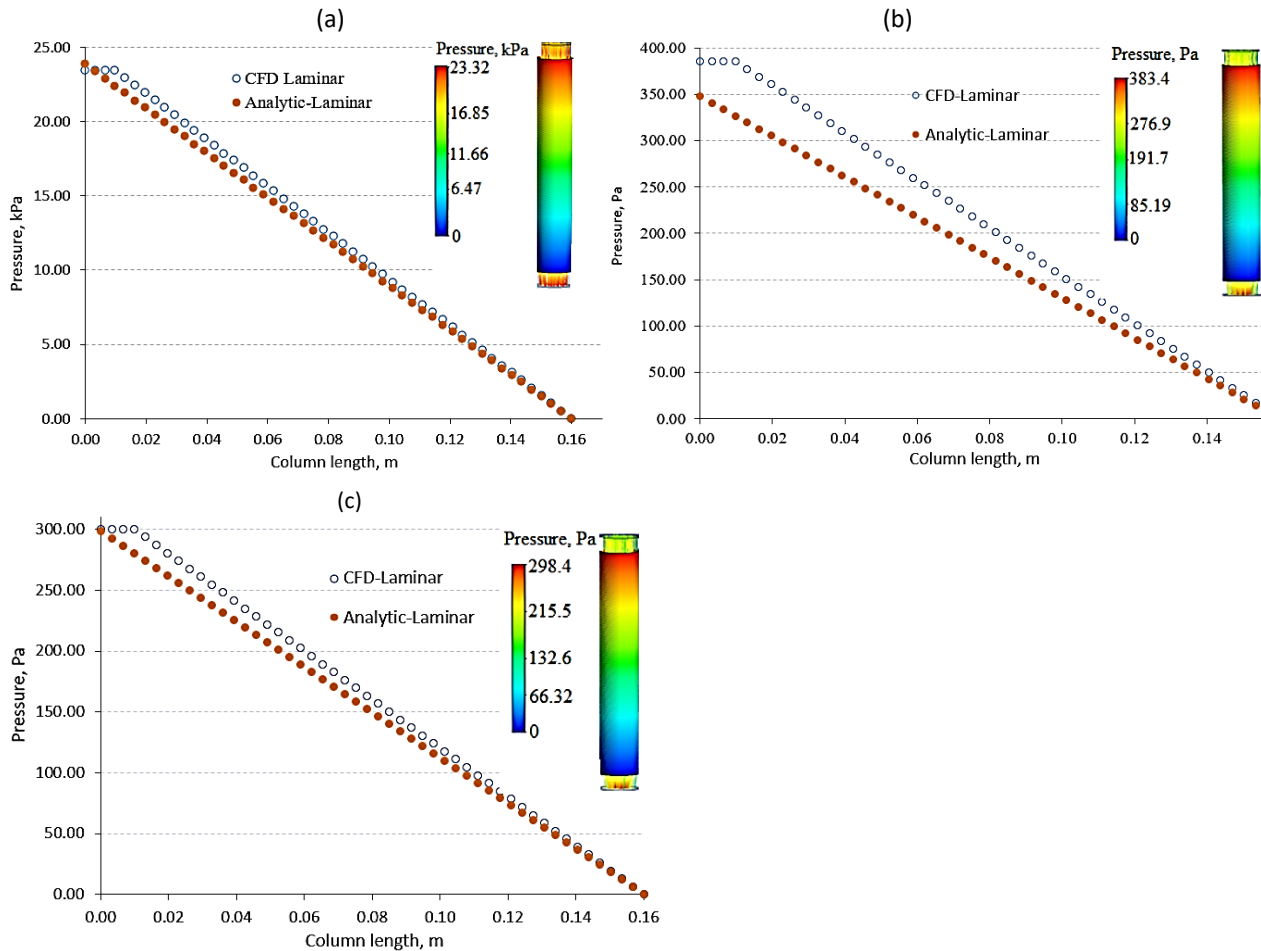

Figure 3. *Pressure variation of (a) water liquid, (b) CO_2, and (c) water vapor flowing through the cylindrical column for a velocity of 0.01 m s^{-1}*

Figure 4 illustrates the distinction in water pressure variations along the column length between laminar flow (inlet velocity of 0.01 m s^{-1}) and turbulent flow regime (inlet velocity of 0.3 m s^{-1}). In the turbulent regime, the CFD model predictions deviated somewhat from the second theoretical term of the Blake-Kozeny equation (analytical solution).

This finding was supported in literature [40] reporting a significant divergence between the numerical and experimental results when compared to empirical correlations in the turbulent regime. The notably higher pressure experienced during turbulent flow, as opposed to laminar flow, signifies that turbulent flow encounters greater resistance and obstruction as water traverses through the system. Conversely, the lower pressure in laminar flow indicates smoother water movement with reduced resistance and obstruction compared to turbulent flow. This is a well-known characteristic of the laminar regime as regular and uniform fluid motion results in a decreased momentum transfer and consequently a lower pressure. The incongruity between the theoretical model for turbulent flow and CFD outcomes suggests potential disparities or constraints within the model's assumptions. Turbulent flows entail intricate phenomena such as turbulent eddies, vortex shedding, and other complex fluid behaviors, which can pose challenges in accurately capturing them within a theoretical framework. Conversely, CFD simulations employ robust numerical techniques to solve governing equations, offering more detailed and realistic portrayals of turbulent flows. The disparity between the theoretical model for turbulence and CFD model implies potential refinements that may be necessary in the theoretical model's formulation to align with empirical observations.
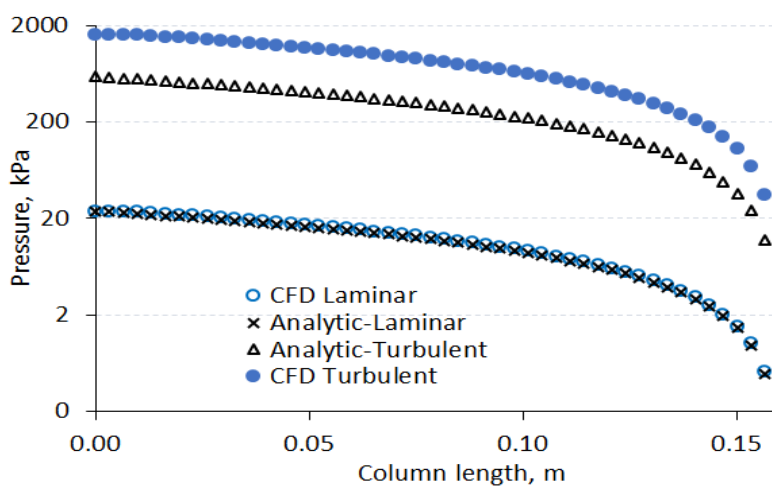

Figure 4. *Comparison of pressure variations in a logarithmic scale over the column length for water flow in laminar and turbulent regimes (inlet velocities 0.1 and 0.3 m s^{-1}, respectively) predicted by CFD modeling and analytical solutions*

Figure 5 illustrates the pressure variation along the column length for different fluids. Water exhibits a higher pressure compared to CO_2 and vapor, while CO_2 demonstrates a higher pressure than vapor. The increased pressure experienced by water as compared to gases is expected. Factors such as water's viscosity, density, and interaction with the packing material play significant roles in contributing to this elevated pressure.
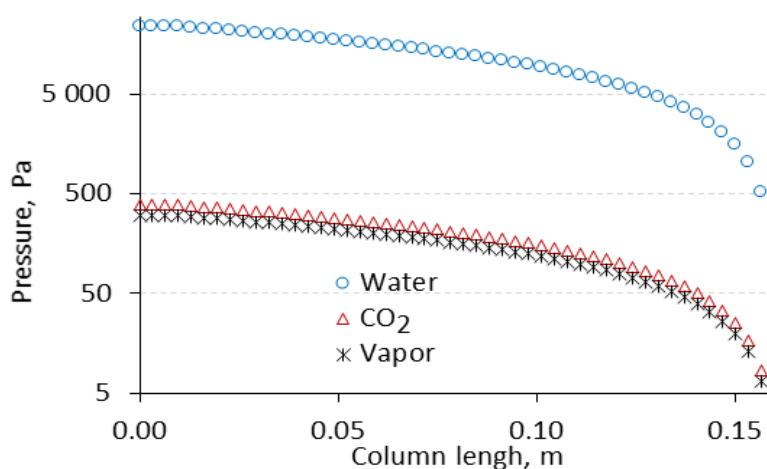

Figure 5. *Comparison of pressure variation in the laminar regime*

In contrast, the pressure for CO_2 is lower than that for water but higher than that for vapor, which registers the lowest pressure among the three fluids examined. Vapor's attributes, including lower viscosity, density, and compressibility, contribute to this diminished pressure. These outcomes underscore distinct flow characteristics and levels of resistance encountered by each fluid within the packed bed column.

3. 2. Turbulent kinetic energy evolution

The Peng-Robinson (PR) equation of state is a widely used thermodynamic model for describing fluid behavior as a function of pressure, volume and temperature, particularly in chemical and petroleum engineering. It offers significantly improved accuracy over the van der Waals equation for predicting the properties of gases and liquids such as nitrogen, carbon dioxide, and hydrocarbons. Because of its reliability and computational efficiency, PR equation is commonly applied to phase equilibrium calculations and prediction of interfacial properties [41].

Figure 6 presents the variation of turbulent kinetic energy (TKE) along the column for three different fluid models: ideal gas, real gas, and a simplified constant-density/viscosity (CD) gas model. The evolution of TKE offers critical insight into how turbulence responds to differences in fluid properties and modeling assumptions. In the initial region of the column, approximately the first third, all three models display similar TKE magnitudes. This convergence suggests that at the early stage of flow development, turbulence is not significantly influenced by thermodynamic property variations. In this zone, velocity gradients, pressure drops, and thermal effects are still moderate, resulting in comparable flow conditions across the models. As the vapor proceeds downstream, clear divergences emerge. In the CD model, a sharp increase in TKE is observed near z = 0.06 m. This spike stems from the oversimplified assumption of constant density and viscosity, which fails to capture the damping effects of compressibility and temperature-dependent viscosity.
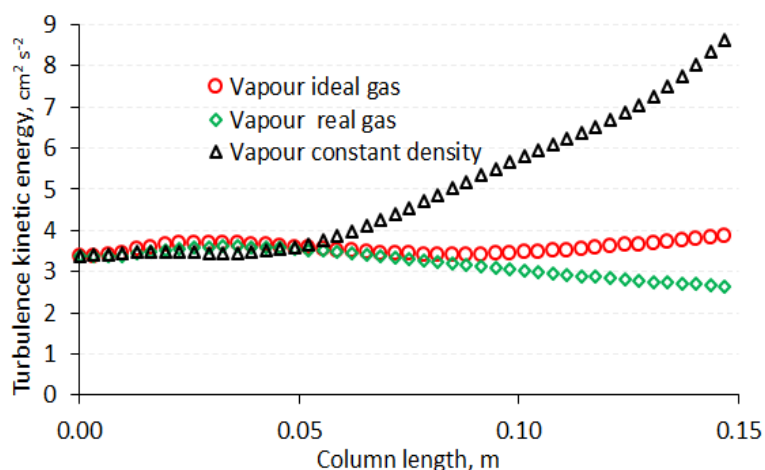

Figure 6. *Turbulent kinetic energy variations in the turbulent regime along the column length for 3 vapor models: ideal gas, real gas, and a constant-density/viscosity (CD) gas*

As a result, the model artificially sustains higher turbulence levels in response to accelerating flow, exaggerating local energy fluctuations. In contrast, the real gas model shows a gradual decrease in TKE toward the column outlet. This behavior reflects the realistic treatment of fluid properties, particularly the pressure-dependent viscosity and density. As pressure drops along the column, the fluid becomes less dense and more viscous, enhancing viscous dissipation and thus reducing turbulent intensity. This highlights the real gas model's ability to capture energy loss mechanisms more faithfully. The ideal gas model presents an intermediate behavior, maintaining relatively stable TKE values along most of the column length. A slight increase near the outlet can be attributed to mild compressibility effects and increased velocity gradients in that region. However, since this model does not account for intermolecular interactions, it underestimates both dissipative and amplifying mechanisms in turbulent transport. In conclusion, a fluid that experiences energy loss during flow is the most physically realistic scenario. Consequently, the PR model emerges as the most appropriate model for simulating real gas behavior. This final result highlights the importance of the PR model, making it the most suitable and reliable among the models considered.

Figure 7 depicts the TKE variation for the three modeled fluids in a turbulent regime along the column length. The TKE is in the following ascending order: vapor>CO_2> water. In the case of water, the TKE exhibits a progressive decline until it reaches the outlet of the column. For CO_2, TKE initially decreases slowly. However, at a column length of 0.035 m, it begins to decrease rapidly until it exits the column. In contrast, the pattern of TKE variation for vapor is markedly different. It resembles the behavior of CO_2 up to a column length of 0.015 m at the inlet, after which TKE experiences a significant increase, attaining elevated values by 0.035 m column length, before subsequently declining progressively until reaching the outlet.
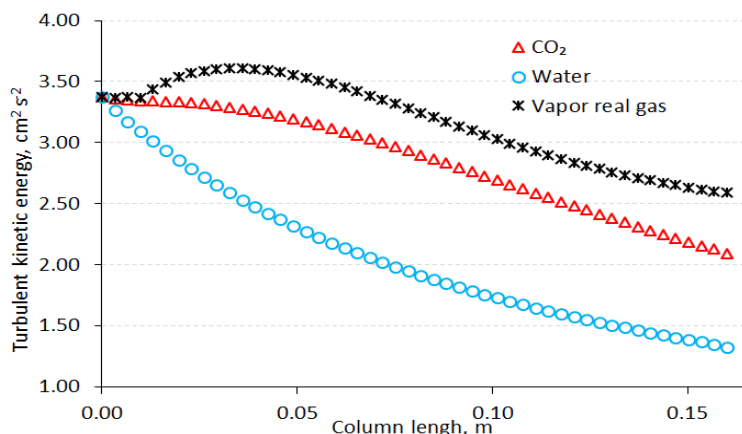

Figure 7. *Turbulent kinetic energy variations along the column length in turbulent flow regime for water, CO_2 and water vapor modeled as a real gas*

3. 3. Evolution of turbulent eddy dissipation

Variations of turbulent eddy dissipation (TED) along the column length for water, water vapor, and CO_2 are shown in Figure 8. A clear disparity in TED behavior is observed among the three fluids. Water exhibits the highest initial TED, which gradually declines along the column, reaching its lowest value at the outlet. This decreasing trend suggests a gradual attenuation of turbulence as the kinetic energy is dissipated through the densely packed porous medium. The high TED at the inlet can be attributed to water's relatively high density and viscosity, which promote stronger inertial forces and shear-induced turbulence as the fluid impinges on the solid matrix. In contrast, both vapor and CO_2 start with lower TED values that progressively increase along the column. These trends, while initially counterintuitive, can be mechanistically linked to the distinct thermophysical properties of each fluid. For vapor, the increase in TED may arise from compressibility effects and potential phase instability under pressure drop. As vapor moves through the packed bed, local pressure drops can induce partial condensation or oscillations around saturation conditions, leading to localized density gradients and transient two-phase regions. These dynamic fluctuations can enhance shear and promote eddy formation, contributing to higher energy dissipation downstream. Additionally, the release or absorption of latent heat during phase change may alter local temperature gradients, reinforcing turbulence through buoyancy-driven instabilities.
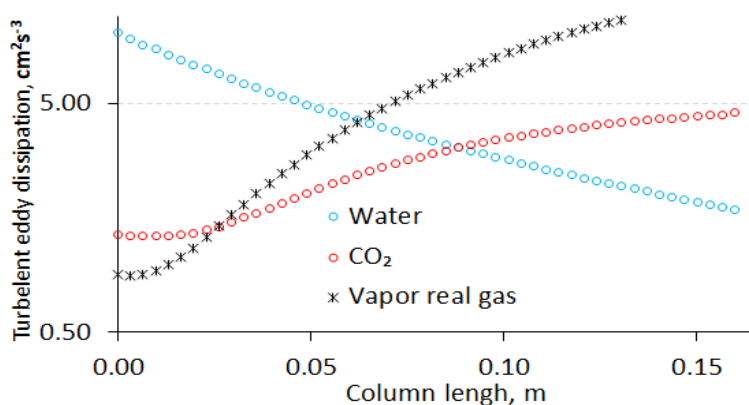

Figure 8. *TED predictions along the column length in turbulent flow regime for water, CO_2 and water vapor modeled as a real gas*

For CO_2, the gradual rise in TED along the column may be attributed to its transition toward or within the supercritical regime [42]. Supercritical CO_2 exhibits a sharp variation in key transport and thermodynamic properties such as density, specific heat capacity, and viscosity near its pseudo-critical point [43]. These elements can increase turbulence intensity by destabilizing the flow and enhancing scalar mixing. In particular, the combination of gas-like diffusivity and liquid-like density promotes efficient momentum and mass transfer, supporting the formation of eddies deeper in the column. However, the manifestation of supercritical or pseudo-critical effects strongly depends on the proximity of the operating conditions to the critical point. In the present study, the pressure distribution along the porous column shows a continuous decrease, which remains several orders of magnitude below the critical pressure of CO_2 [42,43]. Under such conditions, sharp pseudo-critical variations in thermophysical properties are not expected to be activated within the flow domain. Accordingly, the observed gradual increase in TED is more consistently explained by hydrodynamically driven mechanisms inherent to flow through porous media. As pressure decreases along the porous column due to flow resistance, CO_2 behaves as a compressible fluid. Consequently, the associated density reduction combined with pore-scale constrictions, increases the local flow velocity gradients, thereby accelerating the transfer of turbulent kinetic energy to smaller scales, which results in a smooth downstream increase in TED [44]. As a result, the initially lower TED for CO_2 may stem from its relatively low inlet density and viscosity compared to water, resulting in reduced inertial forces and weaker initial turbulence.

Overall, the TED profiles highlight how each fluid's turbulence dissipation behavior is governed by its dominant hydrodynamic characteristics within the porous medium, including momentum exchange in water, phase change induced flow variability in vapor, and compressibility-driven velocity gradients in CO_2.

4. CONCLUSION

Studies using CFD to analyze the movement of water and gases within a packed bed offer significant advantages in understanding flow dynamics, refining design variables, and improving overall system efficiency, depending on the prevailing flow conditions. In laminar flow, water exhibits a relatively constant and organized flow pattern as it passes through the packed bed. This behavior is characterized by a significant increase in pressure, increased turbulence, and maximum energy dissipation. However, CO_2 and steam exhibit relatively lower pressure in both regimes. The TED of CO_2 is relatively high, indicating that this fluid generates less turbulence during its flow through the packed column, and by the same way indicating a less energy dissipation. Vapor modeled as a real gas (Peng-Robinson model) exhibits the highest TED among the three fluids. This implies that vapor displays the lowest turbulent behavior and minimal energy dissipation. Overall, these results highlight the distinct behaviors of water, CO_2, and vapor in both laminar and turbulent flow regimes through a packed bed. Understanding these differences is crucial for designing and optimizing processes that involve these fluids in porous media, such as enhanced oil recovery.

Nomenclature

C_2 / m^{-1}	- Inertial resistance coefficient
d_p / m	- Mean particle diameter
L / m	- Bed length
ΔP / Pa	- Pressure drop
Re	- Reynolds number
u_0 / m s^{-1}	- Linear velocity related to an empty cross-section of the column
u_{in} / m s^{-1}	- Interstitial velocity

Letter Greek

$(1/\alpha)$ / m^{-2}	- Resistance coefficient
ε	- Void fraction (voidage)
μ / Pa s	- Dynamic viscosity
σ / kg m^{-3}	- Density of the fluid

Abbreviations

CD	- Constant density
CFD	- Computational fluid dynamics
PR	- Peng-Robinson
TED	- Turbulent eddy dissipation
TKE	- Turbulent kinetic energy

REFERENCES

[1]   Dong X, Liu H, Chen Z, Wu K, Lu N, Zhang Q. Enhanced oil recovery techniques for heavy oil and oil sands reservoirs after steam injection. *Appl Energy*. 2019; 239: 1190-1211. https://doi.org/10.1016/j.apenergy.2019.01.244

[2]   Zhou X, Wang Y, Zhang L, Zhang K, Jiang Q, Pu H, Wang L, Yuan Q. Evaluation of enhanced oil recovery potential using gas/water flooding in a tight oil reservoir. *Fuel*. 2020; 272: 117706. https://doi.org/10.1016/j.fuel.2020.117706

[3]   Keyvan Hosseini M, Liu L, Keyvan Hosseini P, Bhattacharyya A, Lee K, Miao J, Chen B. Review of hollow fiber (HF) membrane filtration technology for the treatment of oily wastewater: Applications and challenges. *J Mar Sci Eng*. 2022; 10(9). https://doi.org/10.3390/jmse10091313

[4]   Kumar P, Brar SK, Cledon M. A computational fluid dynamics approach to predict the scale-up dimension of a water filter column. *Case Stud Chem Environ Eng*. 2022; 5: 100201. https://doi.org/10.1016/j.cscee.2022.100201

[5]   Brown GO. Henry Darcy and the making of a law. *Water Resour Res*. 2002; 38(7): (11-1)-(11-12). https://doi.org/10.1029/2001WR000727

[6]   Shu X, Wu Y, Zhang X, Yu F. Experiments and models for contaminant transport in unsaturated and saturated porous media-A review. *Chem Eng Res Des*. 2023; 192: 606-621. https://doi.org/10.1016/j.cherd.2023.02.022

[7]   Yan C, Fan H, Huang D, Wang G. A 2D mixed fracture-pore seepage model and hydromechanical coupling for fractured porous media. *Acta Geotech*. 2021; 16(10): 3061-3086. https://doi.org/10.1007/s11440-021-01183-z

[8]   Amini Y, Shadman MM, Karimi-Sabet J. CFD simulation of flow distribution in the randomly packed bed Dixon ring. *Sep Sci Technol*. 2022; 57(12): 1900-1909. https://doi.org/10.1080/01496395.2021.2009513

[9]   Lagrée B, Zaleski S, Bondino I. Simulation of viscous fingering in rectangular porous media with lateral injection and two- and three-phase flows. *Transp Porous Media*. 2016; 113(3): 491-510. https://doi.org/10.1007/s11242-016-0707-x

[10]   Liu S, Liu L, Gu H, Wang K. Experimental study of gas-liquid flow patterns and void fraction in prototype 5 × 5 rod bundle channel using wire-mesh sensor. *Ann Nucl Energy*. 2022; 171: 109022. https://doi.org/10.1016/j.anucene.2022.109022

[11]   Alhosani A, Selem A, Foroughi S, Bijeljic B, Blunt MJ. Steady-state three-phase flow in a mixed-wet porous medium: A pore-scale X-ray microtomography study. *Adv Water Resour*. 2023; 172: 104382. https://doi.org/10.1016/j.advwatres.2023.104382

[12]   Liao Y, Zheng J, Wang Z, Sun B, Sun X, Linga P. Modeling and characterizing the thermal and kinetic behavior of methane hydrate dissociation in sandy porous media. *Appl Energy*. 2022; 312: 118804. https://doi.org/10.1016/j.apenergy.2022.118804

[13]   Chen X, Zhao H. A phenomenological design method of the parallel packed bed reactors for chemical looping combustion of gas fuels. *Chem Eng Sci*. 2024; 292: 119988. https://doi.org/10.1016/j.ces.2024.119988

[14]   Amini Y, Nasr Esfahany M. CFD simulation of the structured packings: A review. *Sep Sci Technol*. 2019; 54(15): 2536-2554. https://doi.org/10.1080/01496395.2018.1549078

[15]   Wang Y. CFD simulation of propane combustion in a porous media: application to enhanced oil recovery of heavy oil reservoirs. *Pet Sci Technol*. 2020; 38(5): 432-439. https://doi.org/10.1080/10916466.2019.1705857

[16]   Jiang Y, Khadilkar MR, Al-Dahhan MH, Dudukovic MP. CFD of multiphase flow in packed-bed reactors: II. Results and applications. *AIChE J*. 2002; 48(4): 716-730. https://doi.org/10.1002/aic.690480407

[17]   Gao X, Zhu YP, Luo ZH. CFD modeling of gas flow in porous medium and catalytic coupling reaction from carbon monoxide to diethyl oxalate in fixed-bed reactors. *Chem Eng Sci*. 2011; 66(23): 6028-6038. https://doi.org/10.1016/j.ces.2011.08.031

[18]   Macfarlan LH, Phan MT, Eldridge RB. Methodologies for predicting the mass transfer performance of structured packings with computational fluid dynamics: a review. *Chem Eng Process - Process Intensif*. 2022; 172: 108798. https://doi.org/10.1016/j.cep.2022.108798

[19]   Wang G, Cai W, Xie L, Zhang X, Wang Y. CFD modeling and simulation of the hydrodynamics characteristics of packed column with structured sinusoidal corrugated sheets packings. *Chem Eng Res Des*. 2022; 183: 56-66. https://doi.org/10.1016/j.cherd.2022.04.038

[20]   Peng J, Yu B, Yan S, Xie L. CFD Modeling and simulation of the axial dispersion characteristics of a fixed-bed reactor. *ACS Omega*. 2022; 7(30): 26455-26464. https://doi.org/10.1021/acsomega.2c02417

[21]   Petrazzuoli V, Rolland M, Sassanis V, Ngu V, Schuurman Y, Gamet L. Numerical prediction of Péclet number in small-sized fixed bed reactors of spheres. *Chem Eng Sci*. 2021; 240: 116667. https://doi.org/10.1016/j.ces.2021.116667

[22]   Pashchenko D, Karpilov I, Mustafin R. Numerical calculation with experimental validation of pressure drop in a fixed-bed reactor filled with the porous elements. *AIChE J*. 2020; 66(5): e16937. https://doi.org/10.1002/aic.16937

[23]   Zhuang YQ, Gao X, Zhu Y ping, Luo Z hong. CFD modeling of methanol to olefins process in a fixed-bed reactor. *Powder Technol*. 2012; 221: 419-430. https://doi.org/10.1016/j.powtec.2012.01.041

[24]   Amini Y, Karimi-Sabet J, Nasr Esfahany M, Haghshenasfard M, Dastbaz A. Experimental and numerical study of mass transfer efficiency in new wire gauze with high capacity structured packing. *Sep Sci Technol*. 2019; 54(16): 2706-2717. https://doi.org/10.1080/01496395.2018.1549076

[25]   Mohanty R, Mohanty S, Mishra BK. Study of flow through a packed bed using discrete element method and computational fluid dynamics. *J Taiwan Inst Chem Eng*. 2016; 63: 71-80. https://doi.org/10.1016/j.jtice.2016.03.025

[26] Liu X, Peng C, Bai H, Zhang Q, Ye G, Zhou X, Yuan W. A pore network model for calculating pressure drop in packed beds of arbitrary-shaped particles. *AIChE J*. 2020; 66(9). https://doi.org/10.1002/aic.16258

[27] Ergun S, Orning AA. Fluid flow through aandomly packed columns and fluidized beds. *Ind Eng Chem*. 1949; 41(6): 1179-1184. https://doi.org/10.1021/ie50474a011

[28] Koekemoer A, Luckos A. Effect of material type and particle size distribution on pressure drop in packed beds of large particles: Extending the Ergun equation. *Fuel*. 2015; 158: 232-238. https://doi.org/10.1016/j.fuel.2015.05.036

[29] Wu J, Yu B, Yun M. A resistance model for flow through porous media. *Transp Porous Media*. 2008; 71(3): 331-343. https://doi.org/10.1007/s11242-007-9129-0

[30] Zeng Z, Grigg R. A Criterion for non-Darcy flow in porous media. *Transp Porous Media*. 2006; 63(1): 57-69. https://doi.org/10.1007/s11242-005-2720-3

[31] Ziółkowska, I, Ziólkowski, D.Modelling of gas interstitial velocity radial distribution over a cross-section of a tube packed with a granular catalyst bed. *Chem Eng Sci*. 1993; 48(18): 3283-3292. https://doi.org/10.1016/0009-2509(93)80212-9

[32] Zou Y, Gu H, Huang A, Zhang M, Ji C. Effects of MgO micropowder on microstructure and resistance coefficient of Al2O3-MgO castable matrix. *Ceram Int*. 2014; 40(5): 7023-7028. https://doi.org/10.1016/j.ceramint.2013.12.030

[33] Khalladi R, Benhabiles O, Bentahar F, Moulai-Mostefa N. Surfactant remediation of diesel fuel polluted soil. *J Hazard Mater*. 2009; 164(2-3): 1179-1184. https://doi.org/10.1016/j.jhazmat.2008.09.024

[34] Matsson JE. An introduction to ANSYS fluent 2022. SDC Publications; 2022. https://www.sdcpublications.com/Textbooks/Introduction-ANSYS-Fluent-2022/ISBN/978-1-63057-569-4/

[35] Baker TJ**.** Mesh generation: art or science?. *ProgAerosp Sci.* 2005; 41(1):29-63. https://doi.org/10.1016/j.paerosci.2005.02.002

[36] Hossain MA, Nabavi SA, Ranganathan P, Könözsy L, Manovic V. 3D CFD modeling of liquid dispersion in structured packed bed column for CO_2 capture. *Chem Eng Sci*. 2020; 225: 115800. https://doi.org/10.1016/j.ces.2020.115800

[37] Yang B, Yang T, Xu Z, Liu H, Yang X, Shi W. Impact of particle-size distribution on flow properties of a packed column. *J Hydrol Eng*. 2019; 24(3). https://doi.org/10.1061/(asce)he.1943-5584.0001735

[38] Erdim E, Akgiray Ö, Demir I. A revisit of pressure drop-flow rate correlations for packed beds of spheres. *Powder Technol*. 2015; 283: 488-504. https://doi.org/10.1016/j.powtec.2015.06.017

[39] Linsong J, Hongsheng L, Shaoyi S, Maozhao X, Dan W, Minli B. Pore-scale simulation of flow and turbulence characteristics in three-dimensional randomly packed beds. *Powder Technol.* 2018; 338: 197-210. https://doi.org/10.1016/j.powtec.2018.06.013

[40] Papkov V, Shadymov N, Pashchenko D. Gas flow through a packed bed with low tube-to-particle diameter ratio: Effect of pellet roughness. *Phys Fluids*. 2024; 36(2): 027127. https://doi.org/10.1063/5.0183475

[41] Lopez-Echeverry JS, Reif-Acherman S, Araujo-Lopez E. Peng-Robinson equation of state: 40 years through cubics. Fluid Phase Equilib. 2017; 447: 39-71. https://doi.org/10.1016/j.fluid.2017.05.007

[42] Paterson L, Lu M, Connell L, Ennis-King JP. Numerical modeling of pressure and temperature profiles including phase transitions in carbon dioxide wells. SPE Annual Technical Conference and Exhibition, Denver, Colorado, USA: Society of Petroleum Engineers, 2008, paper SPE-115946-MS. https://doi.org/10.2118/115946-MS

[43] Lv J, Chi Y, Zhao C, Zhang Y, Mu H. Experimental study of the supercritical CO2 diffusion coefficient in porous media under reservoir conditions. R Soc Open Sci. 2019; 6(6). https://doi.org/10.1098/rsos.181902

[44] Skjetne E, Auriault JL. High-velocity laminar and turbulent flow in porous media. *Transp Porous Media*. 1999; 36(2): 131–47. https://doi.org/10.1023/A:1006582211517

Numerička analiza strujanja unutar pakovanog sloja korišćenjem računske dinamike fluida: efekti karakteristika fluida i režima strujanja

Soufiane Ladeg[1,2] i Nadji Moulai-Mostefa[2]

[1]*FST, University of Tissemsilt, Tissemsilt, Algeria*
[2]*LME, University of Medea, Medea, Algeria*

(Naučni rad)

Izvod

U ovom istraživanju primenjena je računska dinamika fluida (engl. computational fluid dynamics - CFD) za poređenje modela strujanja fluida u laminarnom i turbulentnom režimu kroz pakovani sloj. Ispitane su tri vrste fluida (voda, vodena para i ugljen-dioksid). Predviđanja CFD modela su prvobitno upoređena sa dve serije eksperimentalnih podataka objavljene u literaturi. Primećeno je da je korišćeni numerički model u dobroj saglasnosti sa eksperimentalnim podacima, pod uslovom da su dimenzije pakovanog sloja (prečnik i visina kolone, i veličina čestica) u skladu sa onima koje su eksperimentalno korišćene. Model je zatim predvideo opadanje pritiska od vrha kolone do dna u opadajućem redosledu za tri proučavana fluida, za oba režima strujanja. Pored toga, sprovedena je temeljna karakterizacija turbulencije, uključujući određivanje turbulentne kinetičke energije (TKE) i turbulentne disipacije vrtloga (eng.turbulent eddy dissipation - TED). U slučaju vode dobijena je brza disipacija TKE u poređenju sa druga dva fluida, gde se TKE progresivno smanjivala duž kolone. Nasuprot tome, TED za vodu postepeno opada do izlaza iz kolone, dok se za oba gasovita fluida polako povećava duž kolone. Analiza strujanja pare obuhvatila je testiranje dva modela gustine, naime konstantne gustine i Peng-Robinsonovog (PR) modela. Dobijeno je da PR model za svojstva pare pokazuje slične trendove TKE i TED kao u predviđanjima za ugljen-dioksid.